Petroleum Science 19 (2022) 1110–1124

Contents lists available at ScienceDirect

Petroleum Science

journal homepage: www.keaipublishing.com/en/journals/petroleum-science

Original Paper

The mechanism of microwave rock breaking and its potential application to rock-breaking technology in drilling

Ming-Zhong Gao [a, b], Ben-Gao Yang [a, b, *], Jing Xie [b], Si-Qi Ye [b], Jun-Jun Liu [b], Yi-Ting Liu [b], Rui-Feng Tang [b], Hai-Chun Hao [a], Xuan Wang [a], Xiang-Yue Wen [a], Xue-Min Zhou [a]

[a] Guangdong Provincial Key Laboratory of Deep Earth Sciences and Geothermal Energy Exploitation and Utilization, College of Civil and Transportation Engineering, Shenzhen University, Shenzhen, Guangdong, 518060, China
[b] State Key Laboratory of Hydraulics and Mountain River Engineering, College of Water Resource & Hydropower, Sichuan University, Chengdu, Sichuan, 610065, China

ARTICLE INFO

Article history:
Received 26 June 2021
Accepted 21 December 2021
Available online 10 January 2022

Edited by Yan-Hua Sun

Keywords:
Microwave
Well drilling
High efficiency
Granite

ABSTRACT

The exploration and development of oil and gas resources have shifted from shallow to deep and ultradeep. The difficulty of rock breaking has also increased, introducing new challenges to traditional rock-breaking technology. Hence, there is an urgent need to develop new rock-breaking technologies to improve the development efficiency of deep oil and gas resources. Therefore, this study focused on the new microwave rock-breaking technology and conducted experimental and numerical simulation research on typical deep, hard rock granite. The research results showed that granite in the microwave field exhibited high-temperature melting and fracture, and the highest temperature could reach 550 °C. Under the irradiation of circulating microwaves, a minimum irradiation time threshold of 3 min was needed to cause irreversible damage to the rock. The numerical simulation results showed that the interaction of thermal stress and *in situ* stress would cause the inside of the rock stratum to separate into a disturbed deterioration area, disturbed unloading area and initial stress area. These results are expected to provide the necessary technical guidance and theoretical support for the research and development of high-efficiency rock-breaking drilling for deep hard rock.

1. Introduction

The phenomenon of resource exploitation extending to deeper parts of the earth has become increasingly common, and the continuous exploration of the deeper parts of the earth has become an important direction of future scientific and technological innovation in China (Gao et al., 2018, 2020b, 2020c, 2022; Xie et al., 2021). However, the strength of a rock mass also exhibits a nonlinear growth trend with increasing burial depth (Gao et al., 2020d), and the difficulty associated with rock breaking increases gradually. In terms of the drilling method, most polycrystalline diamond compact (PDC) bits are suitable for shallow soft strata (Liu et al., 2021). When faced with deep hard strata, traditional mechanical cutting often experiences problems such as serious tool wear and insufficient invasion, which leads to a sharp increase in the drilling cost and low drilling efficiency (Zhang et al., 2021). As the leading technical support for deep earth development (Gao et al., 2021a), the drilling efficiency will inevitably affect the exploration and development process of deep strata and the development efficiency of deep resources. Research on new theories and methods for efficient rock breaking has become a fundamental scientific problem in the process of deep drilling (Feng et al., 2019; Li et al., 2020). Hence, a new technical means is needed to crack and break hard strata, reduce drilling tool wear, improve drilling efficiency (Xue et al., 2019), and provide technical support for deep earth development and deep resource acquisition (Gao et al., 2021b). Microwave technology is a promising rock-breaking method because of its high efficiency and lack of secondary pollution (Wei et al., 2019; Zheng et al., 2016). This technology has been considered widely by scholars, and systematic research work

* Corresponding author. Guangdong Provincial Key Laboratory of Deep Earth Sciences and Geothermal Energy Exploitation and Utilization, College of Civil and Transportation Engineering, Shenzhen University, Shenzhen, Guangdong, 518060, China.
E-mail address: yangbgao@126.com (B.-G. Yang).

https://doi.org/10.1016/j.petsci.2021.12.031

has been conducted on the fracture weakening and fracture characteristics of typical hard rock in the microwave field.

Hartlieb et al. (2012) and Lu et al. (2019a, 2019b) examined the influence of microwave power, irradiation time and other factors on the mechanical properties of basalt, and experiments were conducted on microwave-induced cracking of basalt under axial stress using an open microwave-induced cracking device for hard rock. Zheng et al. (2020, 2021, 2017) examined the influence of microwave power and irradiation time on the surface temperature rise, spatial temperature distribution, P-wave velocity, and mechanical properties of gabbro, monzonite and granite, and then defined the fracturing index to evaluate the fracture characteristics of rocks in the microwave field. Peinsitt et al. (2010) and Hartlieb et al. (2016) discussed the influence of the thermophysical properties and water-bearing state of basalt, granite and sandstone on their fracture characteristics in a microwave field. Kahraman et al. (2020) studied the influence of microwave irradiation on the uniaxial compressive strength and Brazilian splitting strength of nine igneous rocks. They explained the different characteristics of strength degradation in a microwave field from a mineralogical point of view. Deyab et al. (2020) systematically studied the influence of microwave irradiation on Canadian kimberlite and used the Cerchar abrasively index (CAI) to discuss the abrasiveness of samples. Whittles et al. (2003) and Ali and Bradshaw. (2009, 2010) established a microwave absorbing–nonabsorbing rock model based on numerical simulations. They discussed the thermal damage characteristics of mineral particles in the microwave field and considered that microwave power density is very important for rock crushing. Hence, they recommended the use of high-power microwaves for rock crushing.

The existing exploration results show that the scientific research on granite reservoirs is an important field of oil and gas exploration (Liang et al., 2018; Yang et al., 2021), where granite reservoirs accounted for approximately 40%, and other reserves accounted for 75% (Editorial, 2017). Buried hills with burial depths greater than 4000 m have gradually become an important new direction in the exploration of petroliferous basins (Amorus, 1960; Chung-Hsiang, 1982). Therefore, considerable research has been conducted on the deterioration behavior of granite in the microwave field and the feasibility of cutting and breaking rock using a microwave combined drilling rig. Hu et al. (2019) studied different granite strength degradation behavior caused by microwave and conventional heating. They suggested that microwave irradiation should be used to break the rock in practical applications. Nicco et al. (2020) discussed the role of mineralogy and structure in the microwave pyrolysis of granite from a micro perspective. They suggested that microwaves have the potential to crack and weaken granite. Zeng et al. (2019) and Bisai et al. (2020) showed that microwaves could cause the internal water of granite to evaporate and initiate quartz phase transformation, thereby producing thermal cracks and melting characteristics, resulting in a significant decrease in tensile strength and compressive strength (by 26%). Swart and Mendonidis. (2013) and Menzhulin and Makhmudov. (2019) evaluated the fracture characteristics of granite after microwave irradiation and discussed the relationship between the fracture characteristics of granite in the microwave field and microwave heating temperature. Toif et al. (2017) established a three-dimensional numerical model for the microwave heating of granite samples, evaluated the temperature field and stress field of granite in the microwave field, and discussed the industrial applicability of microwaves for promoting rock fragmentation. Hassani et al. (2016) examined how the microwave power, irradiation time, and distance between the sample and microwave feed port affect the weakening of granite in the microwave field. They established a surface microwave irradiation model with finite element software, which confirmed the feasibility of microwave application in rock breaking. Shepel et al. (2018) used a multiple regression analysis method to discuss the influence of microwave parameters on the cutting force of granite. They reported that the cutting force of granite decreased significantly after microwave irradiation. Lek and Thiti (2009) studied the effect of a low-power (600/800 W) microwave treatment on the compressive strength and cutting rate of granite. They reported that the compressive strength and cutting rate of granite decreased by 70% and 38%, respectively. Lindroth et al. (1993) performed cutting tests with drilling rigs combined with microwaves for basalt and granodiorite and discussed the potential benefits and the optimal application conditions for the combined application of microwave energy and mechanical energy.

In summary, several scholars have conducted systematic studies of the fracture characteristics of granite in a microwave field, discussed the influence of microwave parameters on the mechanical properties of granite, conducted experiments on rock cutting with a microwave combined drilling rig, and demonstrated the industrial applicability of high-efficiency microwave rock breaking from multiple angles and scales. However, few scholars have examined the micro behavior and temperature rise characteristics of different parts of granite after breaking in the microwave field. In addition, there are also few reports on the optimal mode of the microwave feeder arrangement in a drilling rig. Therefore, this study examined typical hard rock granite in deep reservoirs as the research object, analyzed the micro behavior and heating characteristics of different parts of granite in the microwave field, and discussed the feasibility of efficient fracture of granite in the microwave field. Based on COMSOL finite element software, a drilling rock-breaking model integrated with microwaves was established. The influence of factors, such as the high temperature and high stress in deep reservoirs on drilling and breaking rock was considered simultaneously, which provides a reference for the subsequent optimization of drilling the structure design and the construction of indoor simulation experiment platforms.

2. Sample preparation and test methods

2.1. Sample preparation

The granite was taken from Mianning County, Sichuan Province. Fig. 1 shows the results of the lithofacies thin section test. The granite has a sandy, massive structure. The minerals are composed mainly of quartz, plagioclase, alkali feldspar and a small amount of biotite, with a small amount of muscovite and ordinary amphibole. The quartz content and particle size were approximately 29% and 2–4 mm, respectively. The plagioclase content and particle size were approximately 40% and 1–3 mm, respectively. The alkali feldspar content and particle size were approximately 30% and 0.5–3 mm, respectively. The biotite content and particle size were approximately 1% and 0.5–1 mm, respectively. Fig. 2 outlines the processing of granite into $\Phi 50 \times 100$ mm cylindrical specimens. Table 1 lists the basic physical parameters. The density and longitudinal wave velocity were approximately 2.67 g/cm^3 and 3.51 km/s, respectively. In addition, the natural moisture content of granite was obtained by weighing the same batch of rock in the natural state and dry state and obtaining the average value. The mass moisture content of granite was approximately 0.02%.

2.2. Test equipment and methods

The microwave transmitting system is composed of a solid-state microwave source, a circulator, and a cavity. The microwave output power was adjusted from 0 to 1000 W, and the output frequency

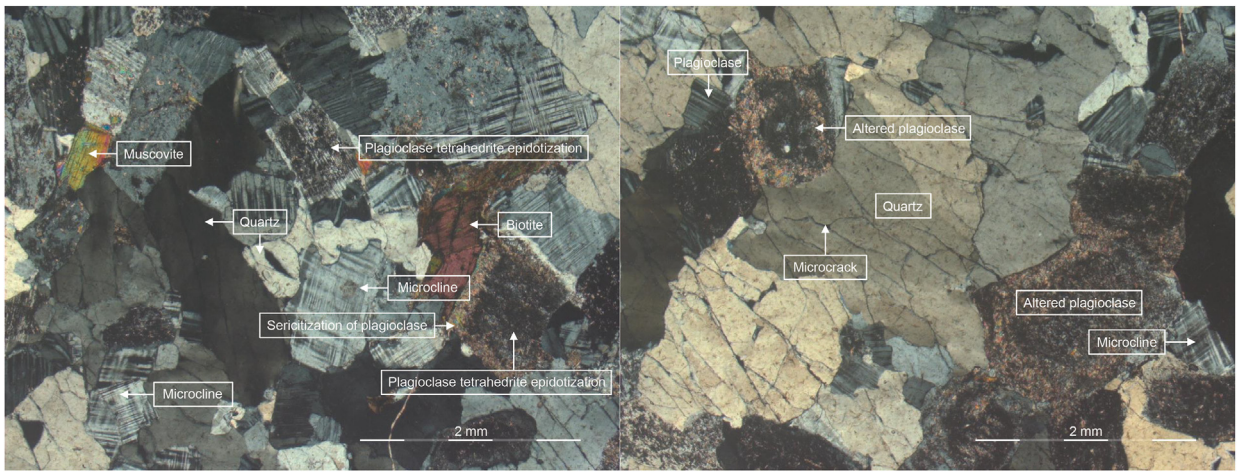

Fig. 1. Lithofacies slice of granite.

Fig. 2. Granite samples.

Table 1
Material parameters of granite samples.

Name	Diameter, mm	Height, mm	Weight, g	Density, g/cm^3	P-wave velocity, km/s
G-1	49.95	100.04	522.11	2.665	3.472
G-2	50.01	100.12	522.21	2.657	3.497
G-3	49.97	99.95	523.33	2.672	3.465
G-4	49.91	100.18	523.18	2.671	3.623

was 2.45 GHz. A non-contact infrared thermometer was used to measure the temperature of the rock surface. The temperature range was from –50 to 700 °C, and the accuracy was ± 2 °C. The rock wave velocity was measured using an I-RPT rock ultrasonic parameter tester. The ranging parameters were set to 100 mm, and the sampling period was 0.2 μs. The transmitting voltage, time window length, and sampling length were 1000 V, 4096, and 1024, respectively. Fig. 3 shows the overall test steps, which are composed mainly of microwave continuous/cyclic irradiation tests. The samples after continuous microwave irradiation are subjected to temperature testing and XRD microanalysis, and the samples after cyclic irradiation are subjected to temperature testing and P-wave velocity testing.

The following two groups of microwave working conditions were employed to study the weakening and fracture characteristics of granite in the microwave field, capture the deterioration law of granite in the microwave field and explore the feasibility of weakening granite in the microwave field: (1) Granite was treated continuously with 1000 W microwave irradiation until the granite was unstable and fractured, and the temperature of the molten and non-molten parts of granite was then measured with a temperature measuring gun. The sample number was G-1. (2) According to the test results of condition 1, cyclic microwave irradiation tests with a rated power of 1000 W and single irradiation times of 2, 3 and

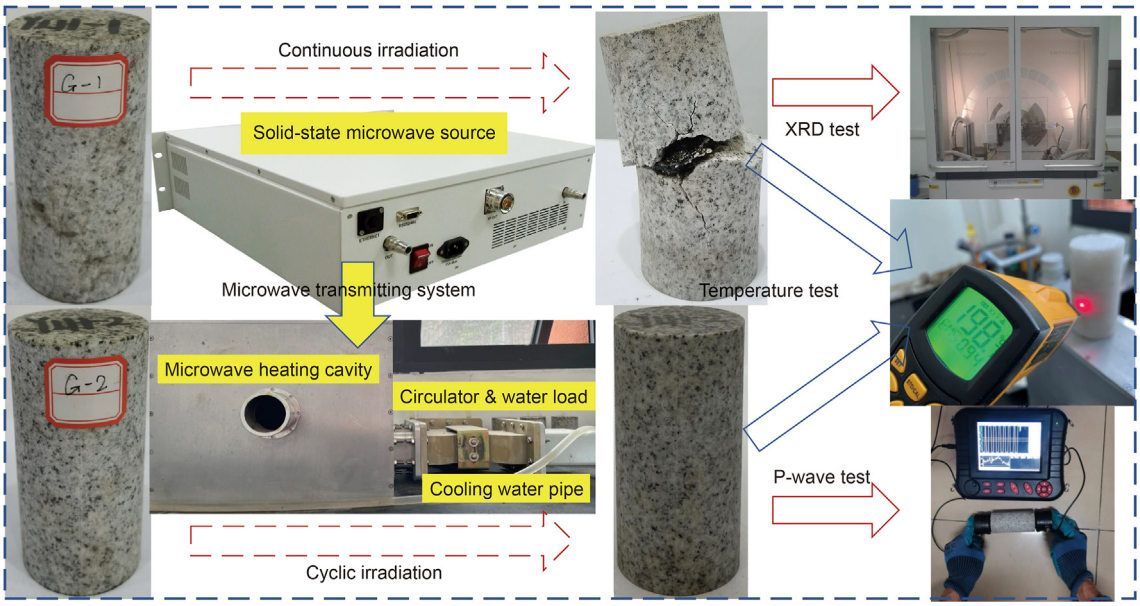

Fig. 3. Schematic diagram of the test system.

4 min were set, and the wave velocity evolution law and heating characteristics of granite in the microwave irradiation process were obtained by infrared temperature measurement and wave velocity testing. The sample numbers were G-2, G-3, and G-4.

3. Study of the macroscopic fracture behavior and microscopic characteristics of granite

3.1. Analysis of the macroscopic fracture characteristics and microscopic behavior of granite under microwave irradiation

Under working condition 1, i.e., when the microwaves act continuously on granite, the experimental phenomenon recorded in the experimental process is as follows. When the microwave irradiated for 4 min 18 s, gas began to escape from the interior. The sample began to emit a local cracking sound when the microwave irradiated for 7 min 44 s. When the microwave irradiated for 11 min 30 s, the gas emitted gradually decreased until the sample cracked from the lower part of the middle part after the microwave irradiated for 12 min 24 s. An analysis of the causes of the test phenomenon and combined with the research results of other scholars (Gao et al., 2020a; Li et al., 2017a; Zeng et al., 2019) suggested that the water in the test changes into water vapor when the internal temperature of the sample reaches a certain level, resulting in the escape of gas in the sample. At the same time, with the continuous input of microwave energy, the thermal damage in the sample intensifies until the sample breaks. Fig. 4 shows the fracture characteristics of the granite after continuous microwave irradiation. After microwave irradiation, the granite appears white near the fracture surface and dark in the initial state far away from the fracture surface. We speculate that the surface of the sample turned white because it was subjected to high temperature action. At the same time, the surface cracks of the sample also showed the radial characteristics of divergence from the fracture to the end of the sample. Based on the chromatic aberration distribution and crack distribution characteristics of the granite surface, the damage of granite is caused mainly by the melting of minerals at high temperatures, which leads to the overall fracture of the sample.

The main factors controlling granite fracture in the microwave

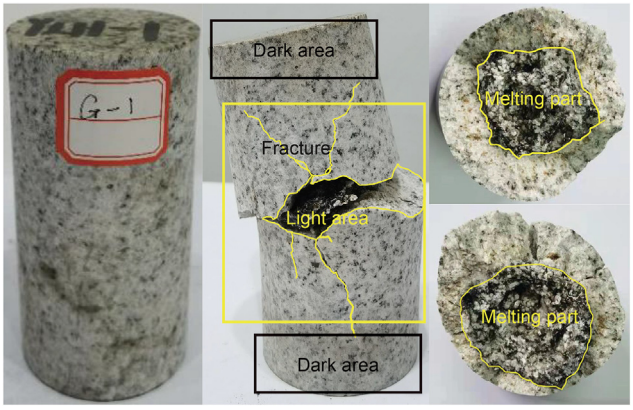

Fig. 4. Fracture diagram of granite in a microwave field.

field were examined further by peeling off the molten part and the non-melted part of the granite; Fig. 5 shows the sampling parts. X-ray diffraction (XRD) and scanning electron microscopy (SEM) were performed. Table 2 lists the XRD test results. The granite is composed mainly of quartz, albite, and muscovite, which is consistent with the test results for the lithofacies thin section. The mineral components of the molten part of granite are mainly quartz and albite, and the main content is quartz, accounting for 85%. The non-molten minerals are composed mainly of quartz, muscovite, and albite at 41%, 36% and 23%, respectively. A comparison of the non-melted and molten mineral components of granite showed that the content of quartz in the molten part was dominant with a small amount of albite and almost negligible calcite and muscovite contents. This result is in sharp contrast to the result for the contents of the non-fused parts of quartz, muscovite, and albite. Therefore, under 1000 W irradiation, the internal temperature of granite increased continuously, and quartz, as a mineral with good thermal expansion and thermal conductivity, melts and flows, continuously concentrating. Finally, it breaks through the constraints of rock to flow out in the form of a molten slurry and form a fracture surface, resulting in a high quartz content of molten

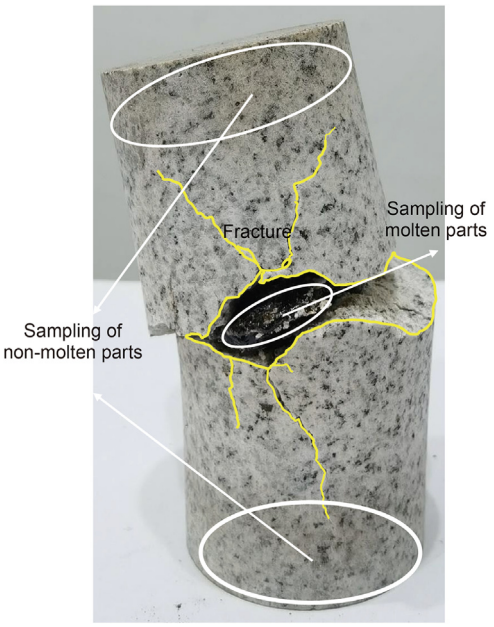

Fig. 5. Sampling diagram.

minerals near the fracture surface. At the same time, the compounds in the sample may also decompose to form quartz under the action of high temperatures. On the other hand, it still shows high-temperature melting failure dominated by quartz.

Fig. 6 shows SEM scanning images of the non-melted part and the molten part of the granite. The non-melted part of the granite was composed mainly of a matrix and cracks (Fig. 6(a)). At the same time, the non-melting part of the granite contained a large number of fracture structures, and the smoothness of the microscopic surface was low (Fig. 6(a)). Fig. 6(b) shows SEM images of the molten part of the granite, which is in sharp contrast to that of the non-melted part. The molten part of the granite contained many microscopic molten pores, and the surface was relatively smooth. The analysis showed that the molten part of granite experienced a high temperature before the sample was destroyed because of the significant selective heating characteristics of microwaves, thereby destroying its internal structure. Hence, the molten part contained many molten pores and smooth a surface on the microscopic scale. The microwave influence on the non-melted part was relatively weak, so the interior was composed mainly of original cracks and structures.

3.2. Exploration of the heating characteristics and degradation behavior of granite in the microwave field

The microwave continuous irradiation test shows that the granite will undergo abrupt changes when microwave irradiated for 4 min 18 s, 7 min 44 s, 11 min 30 s, and 12 min 24 s. One of the elements to ensure the accuracy of measuring P-wave velocity is maintaining an intact sample. Therefore, three groups of test schemes of 4, 3 and 2 min were set up to consider the sample integrity. Fig. 7 shows the temperature measurement process. The temperature measurement principle for complete rock and molten rock is as follows. For the complete rock, some temperature measurements were taken from the bottom to the top. The sample was divided roughly into three parts, and the temperature was measured at two points in each part. By contrast, for the molten rock, the temperature was measured at molten and non-molten parts and 6 points at molten parts. The non-melting part was divided into upper and lower parts, and the temperatures of three sample points were collected at each part. Figs. 8 and 9 shows the temperature rise characteristics of granite under continuous/cyclic microwave irradiation. Fig. 8 presents the temperature evolution characteristics of the non-molten and molten parts during continuous melting fracture of granite, and Fig. 9 shows the evolution characteristics of the maximum temperature, average temperature and minimum temperature of six sample points after a single cycle. The temperature of the molten part and the non-melted part could be distinguished only during continuous irradiation because granite does not appear as molten minerals during cyclic irradiation. The infrared thermometer could only measure the temperature at a fixed point and could not obtain the overall temperature distribution of the sample surface. Hence, the temperature measurement points of each sample were guaranteed to obtain at least six sample points to ensure the validity of the temperature measurement data as much as possible. The temperature of the ruptured surface of the sample under continuous microwave irradiation was significantly higher than that of the non-ruptured surface, as shown in Fig. 8. The maximum temperature was 550 °C, and the maximum temperature difference was 188 °C. Indeed, the measured temperature was only the temperature of the sample surface, owing to the limitations of temperature measurement methods. Moreover, the test failed to capture the temperature distribution inside and on the sample surface under real-time microwave heating. Therefore, the maximum temperature and the maximum temperature difference of granite will be greater than the measured temperature after the microwaves irradiate continuously on the granite. The granite was subjected to the dual coupling effect of high temperatures and thermal stress before being destroyed, i.e., macroscopic melt fracture failure. Fig. 9 shows the law of temperature rises under the irradiation of cyclic microwaves. The sample surface temperature increased with increasing single irradiation time. The temperature rise was smallest when microwaves were applied for 2 min, and it was basically maintained below 200 °C. The temperature was increased further when microwaves were applied for 3 min. Hence, the maximum temperature rise was approximately 250 °C. Based on Figs. 8 and 9, the temperature rises in the cycle test was significantly lower than that

Table 2
XRD test results.

Name	Compound name	Chemical formula	Semi quantitative analysis
Non-molten part	Quartz	SiO_2	41%
	Muscovite	$KAl_{2.2}(Si_3Al)_{0.975}O_{10}((OH)_{1.72}\ O_{0.28})$	36%
	Albite low	$Na(AlSi_3O_8)$	23%
Melting part	Quartz	SiO_2	85%
	Albite low	$Na(AlSi_3O_8)$	14%
	Calcite	$Ca(CO_3)$	1%

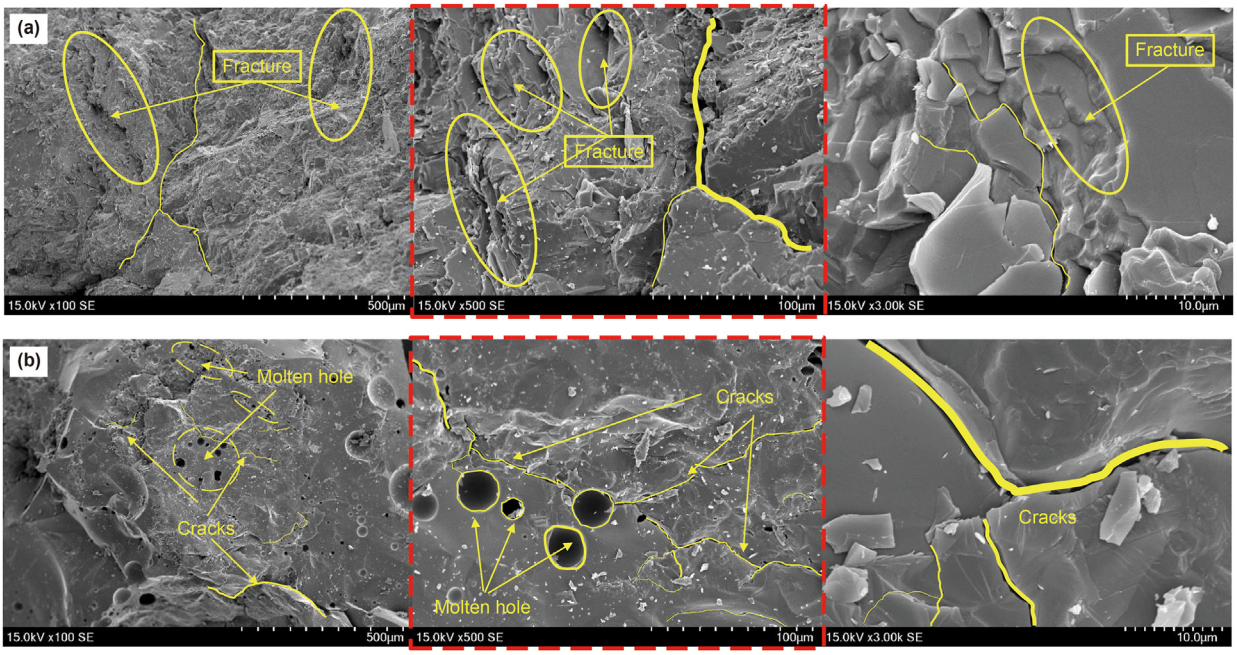

Fig. 6. SEM images of granite. (**a**) SEM image of the non-molten part. (**b**) SEM image of the molten part.

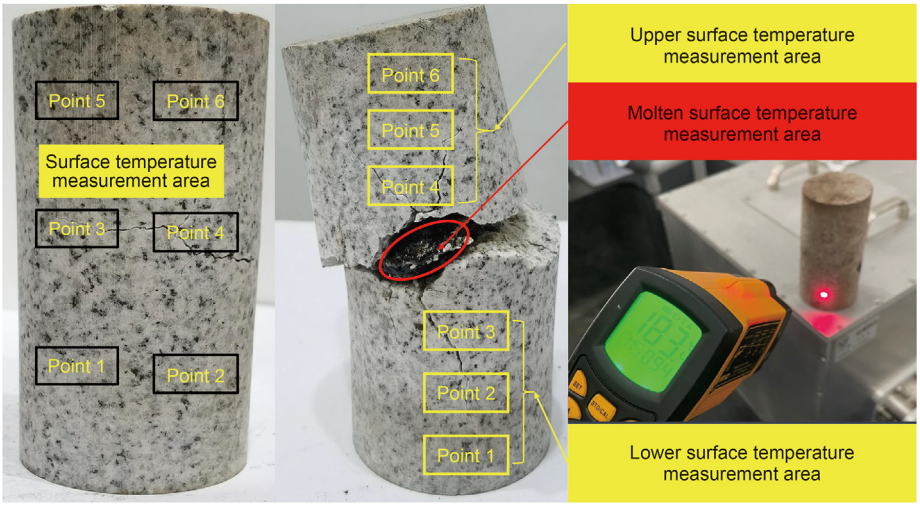

Fig. 7. Schematic diagram of the temperature measurement.

under continuous microwave irradiation. Therefore, the temperature rises under the combined continuous/cyclic microwave irradiation showed that the temperature rise and thermal damage accumulation of the sample increase with increasing single irradiation time. It is not possible to keep irradiating on the sample in engineering practice. Moreover, it is necessary to capture the minimum microwave irradiation time. That is, the rock can be damaged only when the rated microwave power irradiates continuously up to this threshold. In this experiment, when the damaging effect of the sample was evaluated according to the temperature rise, 3 min of single microwave irradiation was the minimum duration threshold of single microwave irradiation.

The rock fracture damage under microwave irradiation was examined quantitatively using the P-wave velocity to characterize the degradation characteristics of granite under cyclic irradiation. The degradation coefficient D_f was defined to eliminate the individual differences in the rocks and compare the degradation characteristics of granite under different single-cycle durations.

$$D_f = \frac{V_{Pi}}{V_{P0}} \tag{1}$$

where D_f is the degradation coefficient; V_{Pi} is the P-wave velocity of sample after microwave irradiation; V_{P0} is the initial P-wave velocity of sample.

Figs. 10 and 11 present the variation law of the P-wave velocity of granite and the degradation coefficient under cyclic microwave irradiation. The degradation coefficient was approximately 0.9 when the duration of single irradiation was 2 min. However, the degradation coefficient reached 0.8 or an even lower value when the time was 3 and 4 min. The P-wave velocity test result was consistent with the temperature measurement result. Hence, a

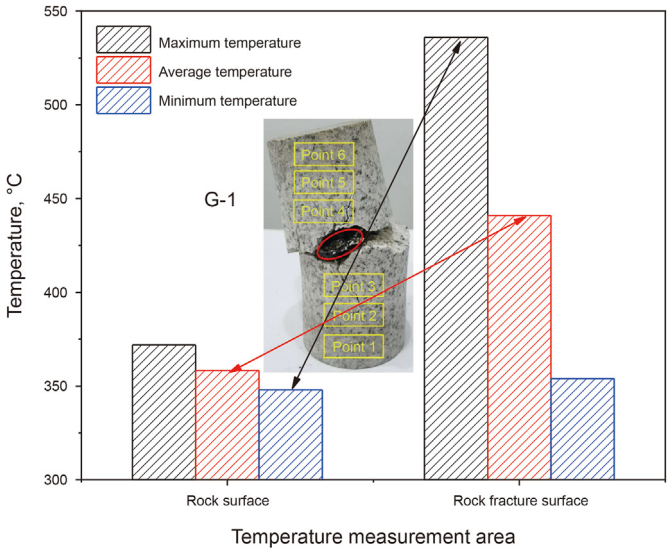

Fig. 8. Temperature rise characteristics of granite under continuous irradiation.

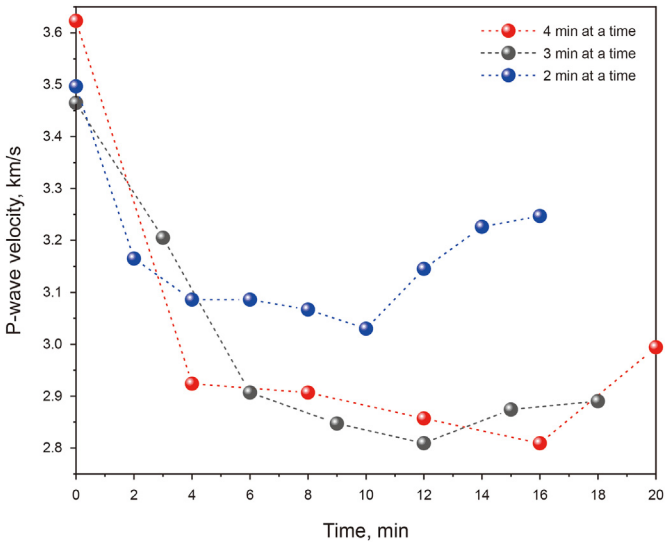

Fig. 10. Evolution characteristics of the P-wave velocity of granite under cyclic irradiation.

certain degree of damage to the specimen will occur when the single-cycle time reaches 3 min, and the damaging effect of rock will be poor after a single 2 min cycle. The temperature measurement and P-wave velocity test show that the granite in the microwave field can reach 200 °C or even higher within a certain time, which will promote the deterioration of granite.

4. Rock-breaking simulation in drilling under microwave irradiation

4.1. Model construction and geometric parameter setting

Research on the fracture characteristics of granite in the indoor-scale microwave field demonstrated the feasibility of granite fractures under microwave irradiation. However, indoor-scale research is still far from meeting the needs of engineering practice, the experimental research and numerical simulation research at engineering scale are still needed. A numerical simulation is favored by scholars because of its high computational efficiency and convenience. In the field of microwave rock breaking, scholars use numerical calculations to compensate for the shortcomings of existing tests and technical means because the existing test methods have difficulty simulating engineering-scale rock breaking. Moreover, it is difficult to explore the distribution characteristics of the electric field, temperature field, and stress field in the test sample by technical means (Hartlieb et al., 2012; Toifl et al., 2016). Microwave drilling combined with rock breaking technology has not been applied to actual engineering on a large scale, and there is no actual engineering model for reference at this stage. Therefore, the model was simplified based on the following assumptions to consider engineering practices and display the electric field, temperature

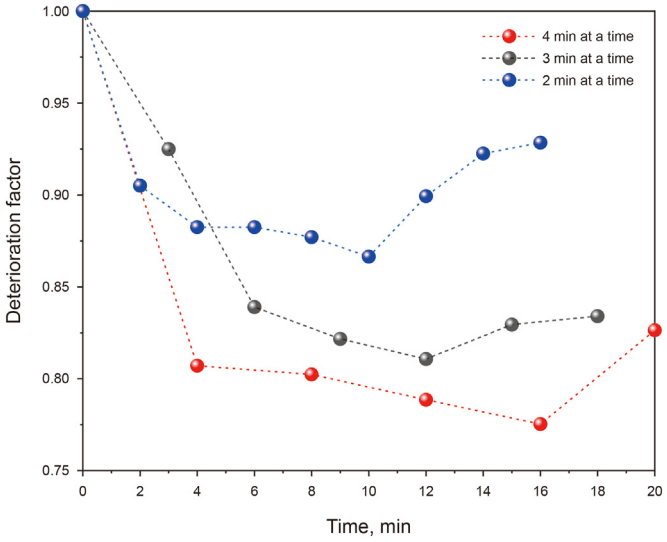

Fig. 11. Evolution characteristics of the deterioration coefficient under cyclic irradiation.

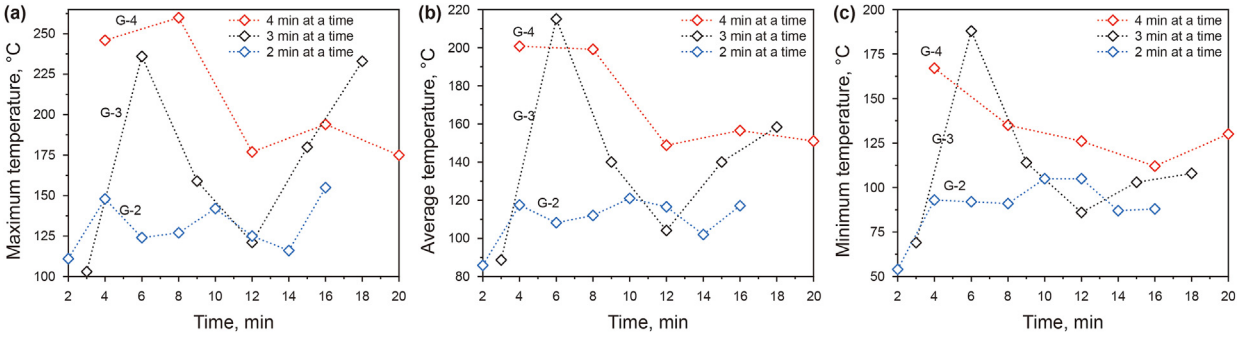

Fig. 9. Temperature rise characteristics of granite under cyclic irradiation. (**a**) Maximum temperature. (**b**) Average temperature. (**c**) Minimum temperature.

field, and stress field of the rock stratum after microwave irradiation more intuitively. (1) The lithology of the target rock stratum is granite, which is a nonmagnetic, homogeneous and isotropic material. (2) The thermodynamic parameters and dielectric constant of granite are fixed values. (3) The chemical reaction and water vapor evaporation effect in the microwave heating process are negligible. (4) Air is a microwave transmission medium, and the dielectric loss is zero. (5) The outer wall of the drill pipe is made from copper with a radius of 50 mm.

Fig. 12 presents the geometric model of microwave drilling. The system is composed of a microwave feed port, an air interlayer, and a rock stratum. The microwave feed port is a BJ 26 rectangular waveguide. The outer wall of the air interlayer is made from copper to simulate the distance between the microwave feed port inside the drilling rig and the drilled rock. Table 3 lists the specific geometric parameters. The thickness of the air interlayer needs to be optimized and adjusted, so the rock stratum is within the high energy threshold because of the short-period oscillating characteristics of microwave propagation in space and to weaken the rock stratum in contact with the drilling rig as much as possible. Therefore, the thickness of the air interlayer was set to z, and the specific value can be expressed as

$$z = \alpha\lambda \tag{2}$$

where α is the thickness coefficient, and the specific value is 0.25–2; λ is the wavelength of the microwave with a frequency of 2.45 GHz, and the value is 12.24 cm.

The model involves three materials: air, copper and granite. The basic material parameters are all taken from the material library. The parameters are listed in Table 4 and expressed as Eqs. (3) and (4):

$$\begin{aligned} k(T) = &-0.00227583562 + 1.15480022\times10^{-4}T \\ &- 7.90252856\times10^{-8}T^2 + 4.11702505\times10^{-11}T^3 \\ &- 7.43864331\times10^{-15}T^4 \end{aligned} \tag{3}$$

$$\begin{aligned} Cp(T) = &\,1047.63657 - 0.372589265T + 9.45304214\times10^{-4}T^2 \\ &- 6.02409443\times10^{-7}T^3 + 1.2858961\times10^{-10}T^4 \end{aligned} \tag{4}$$

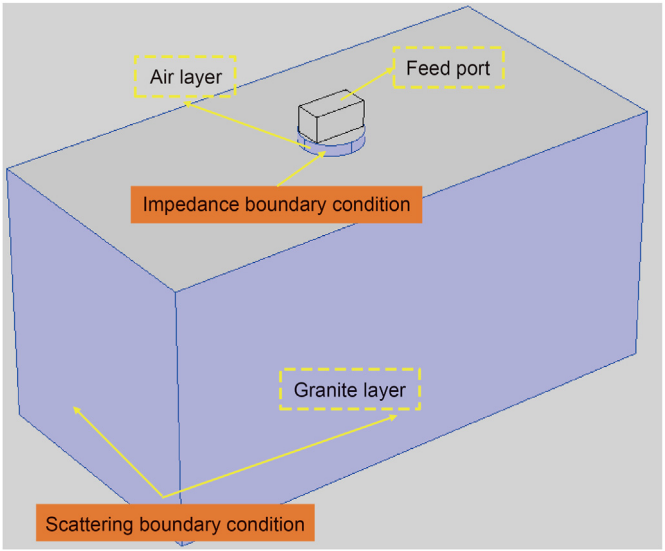

Fig. 12. Rock-breaking model of microwave drilling.

Table 3
Dimensions of the waveguide, air interlayer and granite layer.

	Height, mm	Length, mm	Width, mm	Radius, mm
Waveguide	43.18	86.36	43.18	–
Air interlayer	z	–	–	50
Granite layer	431.8	863.6	431.8	–

Table 4
Thermal and electrical properties of the materials (Liu et al., 2017; Zheng, 2017).

Material properties	Values		
	Air	Copper	Granite
Relative permittivity	1	1	$5.25-0.16j$
Relative permeability	1	1	1
Electrical conductivity, S/m	0	5.998×10^7	0
Thermal conductivity, W/(m·K)	$k(T)$	400	2.9
Density, kg/m^3	ρ	8960	2600
Heat capacity at constant pressure, J/(kg·K)	$Cp(T)$	385	850
Coefficient of thermal expansion, 1/K	–	–	7×10^{-6}

In Table 4, the ρ is the air density function, which was solved by the ideal gas law.

4.2. Governing equations and boundary conditions

The model mainly analyzes the electromagnetic field and heat transfer field, and the electric field intensity of the electromagnetic field is solved using the Helmholtz vector equation (Jiajia et al., 2014):

$$\nabla\times\mu_r^{-1}(\nabla\times\mathbf{E}) - k_0^2(\varepsilon_r - \frac{j\sigma}{\omega\varepsilon_0})\mathbf{E} = 0 \tag{5}$$

where μ_r is the relative permeability; $\mathbf{E}$ is the electric field strength, V/m; k_0 is the free space wave velocity; σ is the conductivity, S/m; ε_r is the dielectric constant; ω is the angular frequency, rad/s; ε_0 is the vacuum dielectric constant, F/m; j is the imaginary part of dielectric constant of materials.

$$k_0 = \frac{\omega}{c_0} \tag{6}$$

where c_0 is the speed of light in a vacuum, 3.8×10^8 m/s.

As a type of dielectric material, when rock interacts with electromagnetic waves, the electromagnetic energy contained in microwaves will be converted to heat energy. Because it was assumed that granite is a nonmagnetic material, the energy absorbed by granite depends mainly on the dielectric loss in the electric field (Jiajia et al., 2014):

$$Q_e = Q_{rh} = \frac{1}{2}Re(\mathbf{J}\cdot\mathbf{E}^*) \tag{7}$$

where Q_e is the electromagnetic power loss, W/m^3, which will be used as a heat source term in the solid heat transfer field to participate in the calculation; Q_{rh} is the resistance loss, W/m^3; Re is the real part of the relative permittivity of materials; $\mathbf{J}$ is the current density, A/m^3.

The electromagnetic power loss is used as a kind of heat source to heat the dielectric material, and solid heat transfer includes two modules of electromagnetic heating and heat conduction, as shown in Eq. (8) (Li et al., 2019):

$$\rho C_p \frac{\partial T}{\partial t} + \rho C_p \mathbf{u} \cdot \nabla T + \nabla \cdot \mathbf{q} = Q_e \tag{8}$$

$$\mathbf{q} = -k \nabla T \tag{9}$$

where ρ is the material density, kg/m^3; C_p is the specific heat capacity at constant pressure, J/(kg·K); T is the absolute temperature, K; $\mathbf{u}$ is the velocity vector of the average movement, m/s; $\mathbf{q}$ is the conduction heat flux density, W/m^2; k is the thermal conductivity, W/(m·K). Eqs. (5)–(9) can be combined to obtain the heating characteristics of dielectric material in a microwave field (Cai, 2002):

$$\varepsilon_{th} = \alpha (T - T_{ref}) \tag{10}$$

$$\sigma_{th} = E \varepsilon_{th} \tag{11}$$

where ε_{th} is the thermal strain; α is the thermal expansion coefficient; T and T_{ref} are the temperatures of the dielectric material and the reference temperature, K, respectively; E is the elastic modulus of the material, GPa.

The thermodynamic response of the rock stratum under microwave irradiation can be discussed using Eqs. (13) and (14).

There are two electromagnetic boundary conditions involved in the microwave propagation process. First, when microwaves propagate in the drill pipe, the drill pipe material defaults to copper metal material. Therefore, the boundary condition is set as the impedance boundary condition (Hong et al., 2016) (Eq. (12)), and the microwaves cannot escape when trapped inside the drill pipe. When the microwave propagates into the rock stratum, the rock stratum needs to be set as an open boundary condition to simulate the real drilling rock-breaking model. The microwave can propagate indefinitely until the attenuation reaches zero. Therefore, the rock boundary is set as the scattering boundary condition (Eq. (13)). In addition, the size of the rock stratum is set to ten times the size of the feed opening to eliminate the influence of the boundary conditions as much as possible. The boundary condition of the temperature field is thermal insulation.

$$\sqrt{\frac{\mu_0 \mu_r}{\varepsilon_0 \varepsilon_r - j\sigma/\omega}} \mathbf{n} \times \mathbf{H} + \mathbf{E} - (\mathbf{n} \times \mathbf{E}) \mathbf{n} = (\mathbf{n} \times \mathbf{E}_s) \mathbf{n} - \mathbf{E}_s \tag{12}$$

$$\mathbf{n} \times (\nabla \times (\mathbf{E})) - jk \mathbf{n} \times (\mathbf{E} \times \mathbf{n}) = 0 \tag{13}$$

where μ_0 is the permeability of the vacuum; σ is the conductivity, S/m; $\mathbf{E}_s$ is the field source vector, k is the wave number.

The user-controlled grid is used for grid division to improve the quality of the grid. As shown in Fig. 13, the average element quality reaches approximately 0.7.

4.3. Research on the optimal layout of the feed opening and the temperature field-stress field of the rock stratum

In the model, the TE_{10} mode microwave with a frequency of 2.45 GHz is excited by a rectangular waveguide and irradiates on the granite layer through the air interlayer. Fig. 14(a) shows the maximum electric field intensity of different air interlayer thicknesses. The overall maximum electric field strength and von Mises stress were attenuated with the increasing thickness of the air interlayer. However, a presplit space is needed to arrange the coring barrel in the actual coring process. Hence, the microwave feed opening needs to reserve a certain space with the bottom of the drill pipe. The variation characteristics of the electric field intensity and stress in the rock stratum with increasing air layer thickness were examined by calculating the relative change rate of electric field intensity and relative change rate of von Mises stress using the following equation:

$$\Delta E_z = \frac{E_z - E_{z-1}}{\Delta \lambda} \tag{14}$$

$$\Delta \sigma_{Mises} = \frac{\sigma_z - \sigma_{z-1}}{\Delta \lambda} \tag{15}$$

where σ_{Mises} is von Mises stress, MPa; ΔE_z and $\Delta \sigma_{Mises}$ are the relative change rate when the thickness of the air interlayer is z; E_z and σ_z are the maximum electric field strength and maximum von Mises stress, respectively, when the thickness of the air interlayer is z; $\Delta\lambda$ is the difference between the thickness of the adjacent air interlayer, with a value of 0.25λ. When $z = 0.25\lambda$ is the initial thickness, it was assumed that ΔE_z and $\Delta \sigma_z = 0$ when $z = 0.25\lambda$. Fig. 14(b) shows the relative change rate of the maximum electric field strength and maximum von Mises stress. When $z = 1.5\lambda$, the relative change rate of the maximum electric field intensity and the maximum von Mises stress were lower, indicating a 1.25λ transition to 1.5λ. The maximum electric field intensity and maximum von Mises stress change relatively little. Therefore, based on a consideration of the attenuation of the electromagnetic field/stress and the relative rate of change, the thickness of the air interlayer is 1.5λ, which is 18.36 cm.

Fig. 15 shows the distribution of the electric field-temperature field-stress field of the granite layer when the thickness of the air interlayer is 18.36 cm. The electric field distribution inside the granite exhibited periodic attenuation characteristics because of the attenuation of microwave propagation in the granite layer and its inherent periodic characteristics. However, the temperature distribution is high in the middle and low in the surroundings because the electric field energy of each cycle is lower than the electric field energy of the previous cycle. The stress field distribution depends mainly on the temperature field distribution, so the stress field distribution presents a bimodal distribution that corresponds to the temperature field distribution.

4.4. Study of the weakening characteristics of the granite layer under microwave irradiation considering the depth effect

From the perspective of resource and energy development trends, the current resource development has entered the deep trend (Gao et al., 2021c; Xie et al., 2020), and the impacts of high ground temperatures and high ground stresses have become more prominent after the project enters the deep part. Therefore, to consider the rock-breaking characteristics of microwave drilling under the influence of the coupling factors of high ground stress and high ground temperature, the following three sets of working conditions were set specifically to simulate the microwave weakening characteristics of granite with a buried depth of 2000 m: (1) A high ground temperature and high ground stress were not considered; (2) only high ground temperature was considered; (3) only high ground stress was considered. According to the geothermal gradient and the distribution of the ground stress (Cai, 2002), the ground temperature was estimated to be 100 °C at a buried depth of 2000 m. In addition, according to the Heim hydrostatic pressure hypothesis, the ground stress was considered a hydrostatic stress state, i.e., $\sigma_h = \sigma_v = \gamma H = 54$ MPa. The ground stress will not affect the electric field strength and distribution because the microwave feed mode, rock size and basic physical and mechanical properties have not been changed. Therefore, only the distribution of the temperature field-stress field of the rock stratum is discussed. The thermal stress inside the rock stratum under

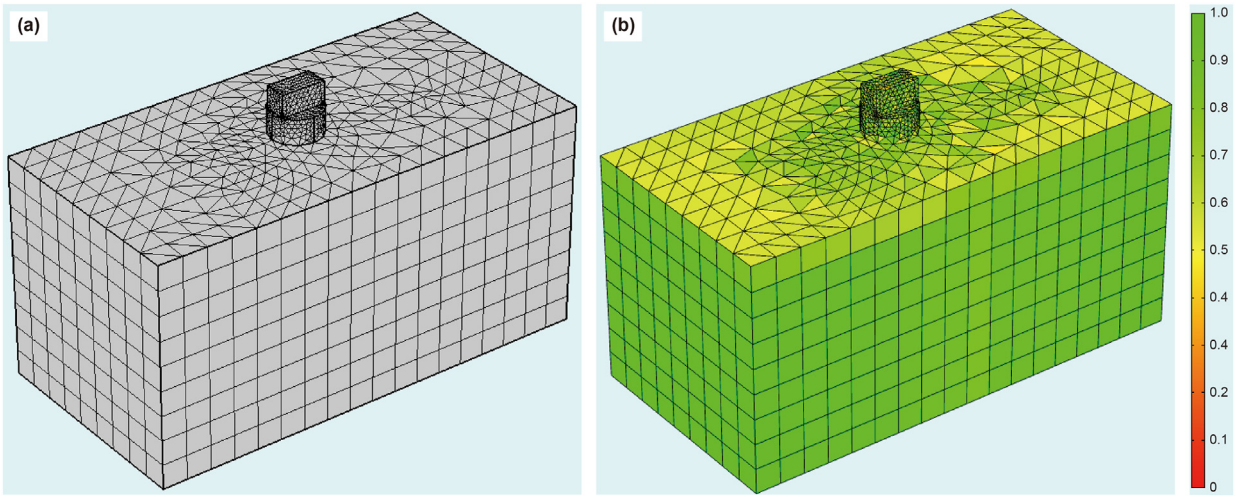

Fig. 13. Model grid diagram. (**a**) Schematic diagram of grid generation. (**b**) Cloud image of the grid quality distribution.

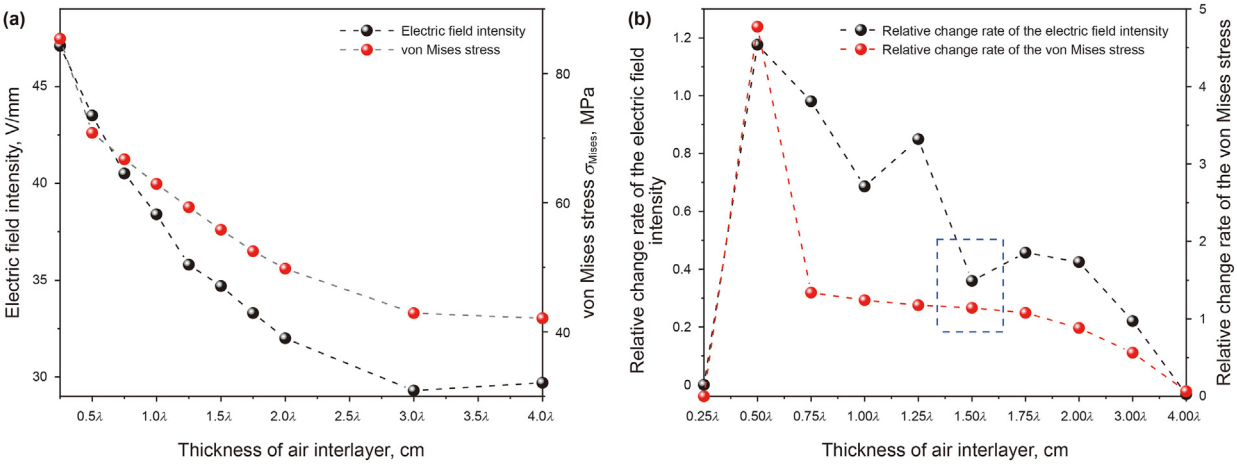

Fig. 14. Electric field strength and von Mises stress of the rock stratum under different air interlayers. (**a**) Maximum electric field intensity and von Mises stress. (**b**) Relative change rate of the maximum electric field intensity and von Mises stress.

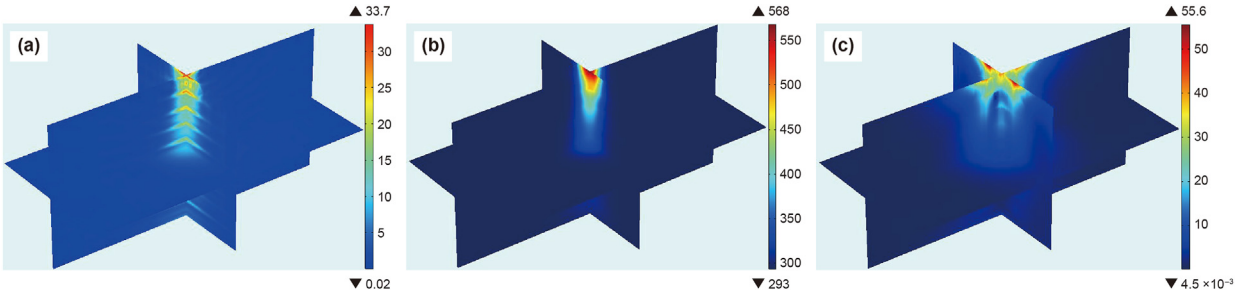

Fig. 15. Multisection diagram of the electric field-temperature field-stress field distribution. (**a**) Electric field (V/mm). (**b**) Temperature field (K). (**c**) Stress field (MPa).

microwave irradiation is caused mainly by the temperature gradient (Eq. (8)). However, the thermal stress will only change its internal physical and mechanical properties when the rock stratum is at a high ground temperature for a long time, while the distribution of the temperature gradients will not change. Therefore, as shown in Fig. 14(a), the high ground temperature under microwave irradiation will not affect the stress field distribution, while the high ground stress state will have a greater impact on the internal stress distribution of the rock stratum. Although the stress adjustment area in Fig. 15(c) is significantly higher than in Fig. 16 (b), the stress adjustment law remains consistent under the two working conditions. Fig. 16(c) shows that higher stress areas are generated in the part closest to the air interlayer, and the stresses exceed 75 MPa. However, a low-stress area appears a certain distance away from the air interlayer, and the stress value is approximately 40 MPa lower than the initial stress, suggesting that the

stress can be released in some rock strata under microwave irradiation.

A typical monitoring line (group) is selected to explore the quantification of the three-dimensional damaged area and the damage evolution characteristics of the rock under microwave irradiation, as shown in Fig. 17. First, the vertical centerline of the granite rock stratum (line 1) is used to quantify the stress evolution characteristics of the granite layer along the depth range. In addition, this provides a reference for selecting line groups 2 and 3 on the *XZ* plane and *YZ* planes, respectively. As shown in Fig. 18, according to the internal stress values and the initial *in situ* stress values in different areas, the granite layer can be divided into three areas along the depth direction after microwave irradiation. When the stress is greater than the initial stress, the granite layer is defined as the disturbed deterioration area (from −66.41 mm to −18.36 mm), with a depth of approximately 48.05 mm. The granite layer is defined as the disturbed unloading area (from −390.26 mm to −66.41 mm) with a depth of 323.85 mm when the stress value is less than the initial stress. Otherwise, it is the initial stress area (from −∞ to −390.26 mm). Based on the results of stress zoning along the depth direction, the stress evolution characteristics of the disturbed deterioration area and the disturbed unloading area are discussed. The disturbed deterioration area is separated was 10 mm, and the disturbed unloading area is separated by 60 mm. The *Z*-axis coordinates were −18.36, −28.36, −38.36, −48.36, −58.36, −68.36, 128.36, −188.36, −248.36, −308.36 and −368.36 mm, denoted by the letter *H*.

Figs. 19 and 20 show the trend of the stress change of monitoring line group 2 and monitoring line group 3. Overall, the stress distribution law is consistent with the stress divisions in Fig. 18. The stress in the disturbed deterioration area was mostly higher than 54 MPa, showing unimodal distribution characteristic. Except for a small part of the disturbed deterioration area, the stress is higher than the initial ground stress, most of which are lower than 54 MPa. Bimodal distribution characteristics were observed, and the stress value experienced a significant drop near the origin. In addition, the influence range of microwave irradiation on the rock stratum decreased from X∈(−200, 200) mm to X∈(−100, 100) mm as the depth of the rock stratum increased, which reduced the range of the influence area by almost half. In particular, there is a large drop in stress near the origin in the disturbed unloading area due to the interaction between the thermal stress and the initial ground stress, which is relatively consistent with the initial ground stress or even lower than the initial ground stress. This suggests that while the microwaves crack and destroy the rock stratum at a close distance, the stress could be simultaneously released to the rock stratum within a certain distance because of their penetrating characteristics, which is more likely to aggravate rock destruction.

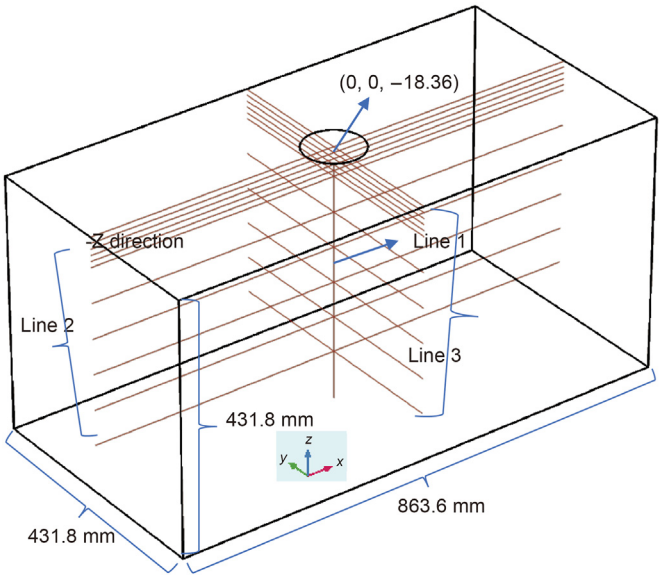

Fig. 17. Schematic diagram of a typical monitoring line selection.

5. Discussion

5.1. Discussion on the fracture mechanism of granite in the microwave field

Previous studies have reported that hard rock in a high-power microwave field will collapse in a short time and at low temperatures, while it will melt at high temperatures for a long time in a low-power microwave field (Li et al., 2017b). Meisels et al. (2015)

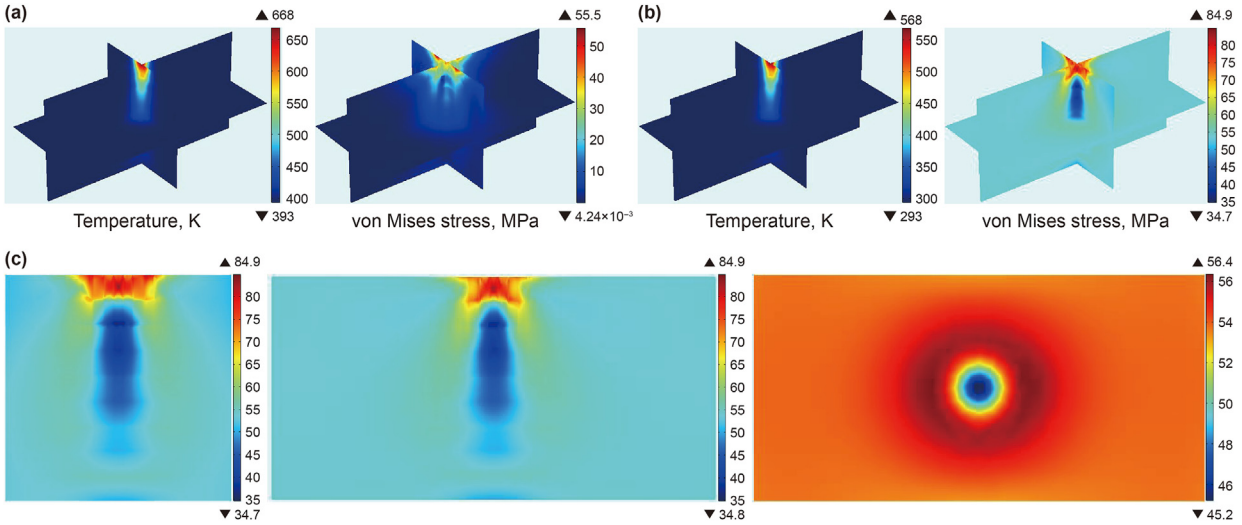

Fig. 16. Distribution of the rock temperature field and stress field under different working conditions. (**a**) Ground temperature is 100 °C. (**b**) *In situ* stress is 54 MPa. (**c**) Stress distribution of each section (54 MPa).

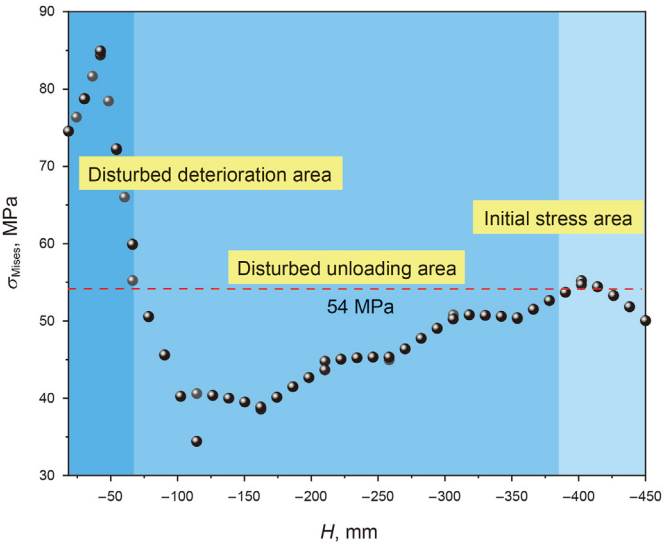

Fig. 18. Stress distribution law of monitoring line 1.

suggested that when the internal temperature of the sample increased rapidly, the internal temperature occurred too late for heat conduction, which led to sharp amplification of the temperature gradient and caused the sample to rupture. Correspondingly, the heat conduction in the sample was relatively sufficient when the microwave power was low, and the temperature stress was unable to increase rapidly in a short time, which led to high-temperature melting failure. In this study, the granite did not crack until approximately 7 min under irradiation with 1000 W microwave power, and it did not break until 12 min. This suggested that under 1000 W microwave irradiation, the internal mineral components of the granite have sufficient time for heat conduction, which extends the length of time that the temperature gradient reaches the tensile limit and promotes the continuous increase in the overall temperature of the sample. Hence, the granite macroscopically presents typical high-temperature melting failure characteristics (Fig. 4).

At the same time, some scholars have interpreted the fracture behavior of quartzite in the microwave field on the micromineral scale. Hartlieb et al. (2012, 2016) and Toifl et al. (2017, 2016) studied quartz α-β. The phase transformation is the main factor in the internal weakening of the rock, and the cracks in the sample are caused by the case where the thermal stress exceeds the tensile limit. Lu et al. (2019a) suggested that rock melting fracture in a microwave field occurs because microwave-sensitive minerals provide heat, thermal expansion minerals provide volume expansion and cracks, and quartz has good thermal conductivity and thermal expansion (Li et al., 2019). The microscopic test results (Table 2 and Fig. 6) showed that the melting part in the microwave field is composed mainly of quartz, and a large number of microcracks and melting holes are generated in the quartz. The fracture of granite is controlled mainly by the phase transformation and melting of quartz.

The above macro- and microlevel analysis suggest that the fracture behavior mechanism of granite under 1000 W microwave irradiation occurs through the following process. Under 1000 W microwave irradiation, there is a specific time for heat conduction inside the granite, leading to thermal stress that does not increase rapidly in a short time. At the same time, the temperature of the quartz minerals continues to rise. Quartz undergoes an α to β phase transformation when the quartz phase transition temperature is reached, which promotes the melting and cracking failure of the sample so that the granite in the microwave field shows the failure characteristics of high-temperature melting.

5.2. Discussion on the feasibility of efficient rock breaking by a microwave combined drilling rig

The numerical results show that under microwave irradiation, different degrees of thermal stress will be produced in the drilled strata, and monitoring line groups 2 and 3 are fitted ($R^2 > 0.9$), as shown in Eq. (16).

$$\sigma_{\text{Mises}} = y_0 + \left(A \Big/ \left(w \times \sqrt{\pi/2}\right)\right)^{-2\times((x-x_c)/w)^2} \tag{16}$$

where y_0, x_c, A, and w are empirical coefficients, which are related to the depth of the monitoring line; x is the independent variable, corresponding to the x coordinate or y coordinate of each point on the line. The equation shows that the stress distribution along the x and y directions on the xy plane of the stratum has a Gaussian distribution. Hence, for the specific xy plane of rock, microwave

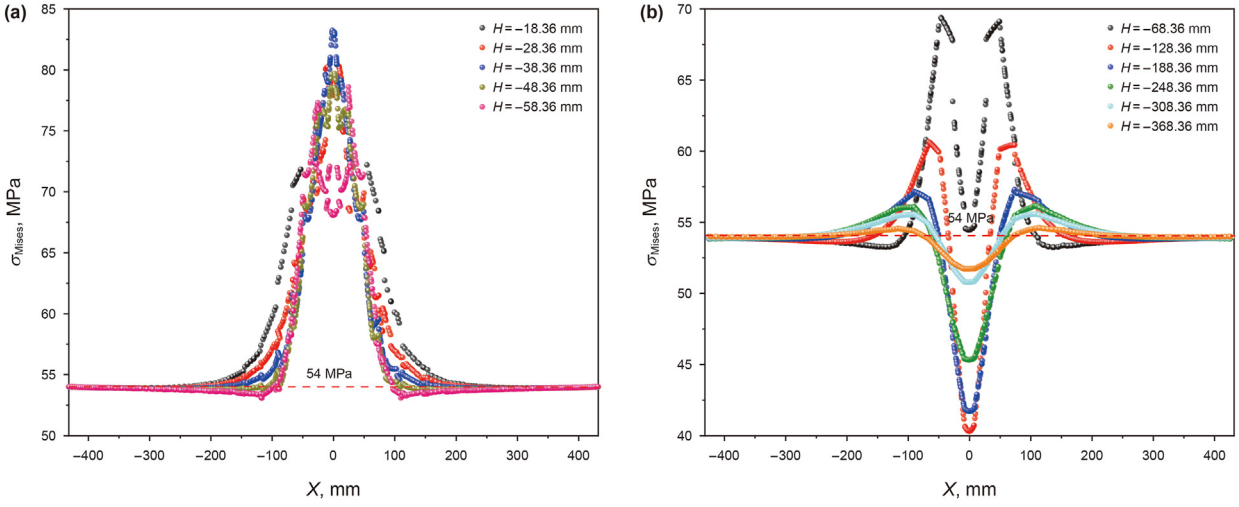

Fig. 19. Stress distribution characteristics of monitoring line group 2. (**a**) Disturbed deterioration area (-58.36 mm $\leq H \leq -18.36$ mm). (**b**) Disturbed unloading area (-368.36 mm $\leq H \leq -68.36$ mm).

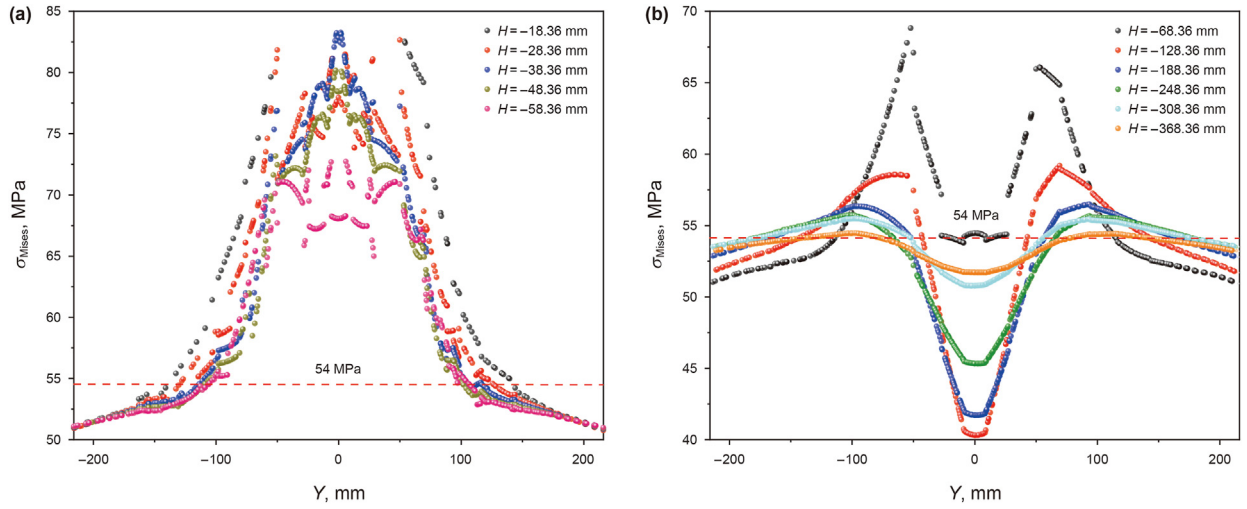

Fig. 20. Stress distribution characteristics of monitoring line group 3. (**a**) Disturbed deterioration area (-58.36 mm $\leq H \leq -18.36$ mm). (**b**) Disturbed unloading area -368.36 mm $\leq H \leq -68.36$ mm.

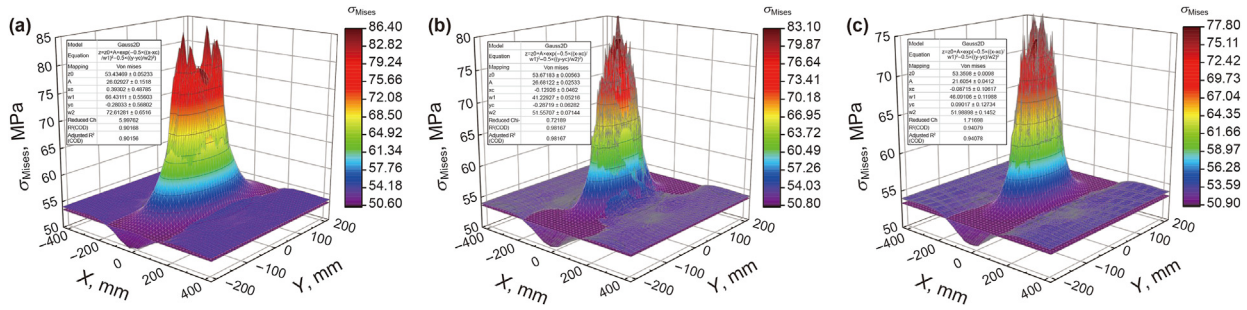

Fig. 21. Stress distribution characteristics on the *xy* plane. (**a**) $H = -18.36$ mm. (**b**) $H = -38.36$ mm. (**c**) $H = -58.36$ mm.

irradiation will produce a high-stress area in a part of that area. This area is the weakening fracture area of rock, which is conducive to drilling machine cutting. Therefore, the damaged area in the *xy* plane of the disturbed deterioration area was characterized quantitatively by selecting three height planes of $H = -18.36$ mm, $H = -38.36$ mm and $H = -58.36$ mm to describe the damaged area. As shown in Fig. 21, a higher stress field is generated in the middle part of the plane, which shows a Gaussian distribution. The surface was fitted to a Gaussian function to describe the electric field distribution of the surface quantitatively ($R^2 > 0.9$), as shown in Eq. (17)).

$$\sigma_{\text{Mises}} = Z_0 + A^{-0.5\times((x-x_c)/w_1)^2 - 0.5\times((y-y_c)/w_2)^2} \tag{17}$$

where the empirical coefficients Z_0, A, x_c, w_1, y_c, and w_2 are related to the distance between the *xy* plane and the microwave feed port. Fig. 21 and Eq. (20) show that when microwaves are applied to the area with initial geostress, the weakening degree of the rock strata in the disturbed deterioration area in front of the drilling rig presents the characteristics of a Gaussian distribution. According to the model in this paper, the range of the strong weakening area is approximately 200 mm^2 with the center of the drill pipe circle. The strong weakening area was approximately equal to the cutting range of the drilling rig. Hence, the microwave combined drilling rig is theoretically feasible.

In terms of the development level of high-efficiency rock-breaking equipment of microwave combined drilling rigs, several studies (Nekoovaght and Hassani, 2014; Wang et al., 2013; Zhang et al., 2014) have reported the possibility of cooperative drilling with combined microwave drilling rigs, which are composed mainly of cutting teeth and microwave generators arranged at the bottom of the drill bit. After the microwave generator is powered on, the transformer increases the voltage. The microwaves are

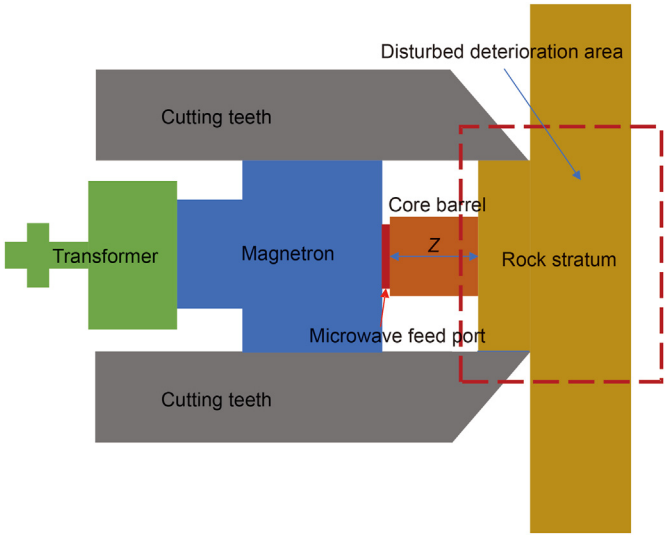

Fig. 22. Schematic diagram of rock breaking using a microwave combined drilling machine (Zhang et al., 2014).

excited by the magnetron tube to heat the rock stratum that is to be drilled and weaken the rock stratum through the generated thermal stress. Subsequently, the cutting teeth break the rock, and the drilling fluid washes the broken particles away from the rock. The rock-breaking schematic diagram was adjusted to show the rock-breaking characteristics of the microwave combined drilling rig more clearly, as shown in Fig. 22, thereby considering the layout of the core barrel and the rock damaged area in front of microwave irradiation. From the perspective of the equipment development, the high-efficiency rock breaking of microwave combined drilling rigs is feasible.

6. Conclusions

In this paper, granite was selected as the research object. Combined with a microwave fracturing test and drilling rock-breaking model, the temperature rise characteristics, fracture characteristics, and degradation behavior of granite in the microwave field were studied from micro to macro perspectives. At the same time, the distribution of the temperature and stress fields in the drilled strata after microwave irradiation was discussed.

(1) Under irradiation at a microwave power of 1000 W, the granite in the microwave field mainly presented the characteristics of high-temperature melt fracture. The maximum monitoring temperature was 550 °C, and radial cracks were formed around the fracture surface. The melting part was composed mainly of quartz and albite, and the fracture morphology was smoother than that of the non-melting part, which was composed mainly of melting holes and cracks.
(2) The cyclic cracking test revealed a minimum irradiation time for thermal damage of granite under microwave irradiation. The temperature rise of the granite surface was small, and the deterioration characteristics were not obvious below this time. In this test, the minimum irradiation time of 1000 W microwave power was 3 min.
(3) The numerical simulation results showed that the distance between the microwave feed port and the drilled strata would affect the thermal damage degree inside the strata. The layout of the core barrel and other modules in engineering practice was considered. Hence, it will be necessary to optimize the layout of the microwave feed port. When a rectangular waveguide is used to excite the TE_{10} mode microwave, it should be 18.36 cm away from the drilled strata.
(4) In the process of deep resource drilling and exploration, the high ground temperature under the irradiation of microwaves will not affect the generation of thermal stress. However, the interaction of *in situ* stress and thermal stress makes the internal stress of the rock stratum adjust to form a disturbed deterioration area and a disturbed unloading area.

Availability of data and material

The raw/processed data required to reproduce these findings cannot be shared at this time as the data also forms part of an ongoing study.

Declaration of competing interest

The authors declare that they have no known competing financial interests or personal relationships that could have appeared to influence the work reported in this paper.

Acknowledgements

This work was financially supported by National Natural Science Foundation of China (U2013603; 52004167), Program for Guangdong Introducing Innovative and Enterpreneurial Teams (No. 2019ZT08G315) and China Postdoctoral Science Foundation (2021T140485).

References

Ali, A.Y., Bradshaw, S.M., 2009. Quantifying damage around grain boundaries in microwave treated ores. Chem. Eng. Process 48 (11–12), 1566–1573. https://doi.org/10.1016/j.cep.2009.09.001.
Ali, A.Y., Bradshaw, S.M., 2010. Bonded-particle modelling of microwave-induced damage in ore particles. Miner. Eng. 23 (10), 780–790. https://doi.org/10.1016/j.mineng.2010.05.019.
Amorus, K., 1960. Petroleum resources in basement rocks. AAPG Bull. 44 (10), 1682–1691. https://doi.org/10.1306/0BDA622D-16BD-11D7-8645000102C1865D.
Bisai, R., Palaniappan, S.K., Pal, S.K., 2020. Influence of individual and combined pretreatment on the strength properties of granite and sandstone. Arabian J. Geosci. 13 (1), 1–10. https://doi.org/10.1007/s12517-019-5009-5, 7.
Cai, M.F., 2002. Rock Mechanics and Engineering. Science Press, Beijing (in Chinese).
Chung-Hsiang, P., 1982. Petroleum in basement rocks. AAPG Bull. 66 (10), 1579–1643. https://doi.org/10.1306/03b5a994-16d1-11d7-8645000102c1865d.
Deyab, S.M., Rafezi, H., Hassani, F., Kermani, M., Sasmito, A.P., 2020. Experimental investigation on the effects of microwave irradiation on kimberlite and granite rocks. J. Rock Mech. Geotech. Eng. 13 (2), 267–274. https://doi.org/10.1016/j.jrmge.2020.09.001.
Editorial, D., 2017. Chinese experts obtain oil through drilling in the granite of Bongor basin in Chad and win the International Award, 001 Chin. Geol. 44, 198–199 (in Chinese).
Feng, J., Shang, L., Li, X., Luo, P., 2019. 3D numerical simulation of heterogeneous in situ stress field in low-permeability reservoirs, 05 Petrol. Sci. 16, 3–19. https://doi.org/10.1007/s12182-019-00360-w.
Gao, F., Shao, Y., Zhou, K., 2020a. Analysis of microwave thermal stress fracture characteristics and size effect of sandstone under microwave heating. Energies 13 (14), 3614. https://doi.org/10.3390/en13143614, 3611-3615.
Gao, M.Z., Chen, L., Fan, D., Yang, M.Q., Liu, C., Li, J.N., Zhao, L., Tian, D.Z., Li, C., Wang, R.Z., Xie, H.P., 2021a. Principle and technology of coring with *in-situ* pressure and gas maintaining in deep coal mine. J. China Coal Soc. 46 (3), 885–897. https://doi.org/10.13225/j.cnki.jccs.YT21.0297 (in Chinese).
Gao, M.Z., Hao, H.C., Xue, S.N., Lu, T., Cui, P.F., Gao, Y.N., Xie, J., Yang, B.G., Xie, H.P., 2022. Discing behavior and mechanism of cores extracted from Songke-2 well at depths below 4,500 m. Int. J. Rock Mech. Min. Sci. 149, 104976. https://doi.org/10.1016/j.ijrmms.2021.104976.
Gao, M.Z., Wang, M.Y., Xie, J., Gao, Y.N., Deng, G.D., Yang, B.G., Wang, F., Hao, H.C., Xie, H.P., 2020b. *In-situ* disturbed mechanical behavior of deep coal rock. J. China Coal Soc. 45 (8), 2691–2703. https://doi.org/10.13225/j.cnki.jccs.2020.0784 (in Chinese).
Gao, M.Z., Liu, J.J., Lin, W.M., Deng, G.D., Peng, G.Y., Li, C., He, Z.Q., 2020c. Study on in-situ stress evolution law of ultra-thick coal seam in advance mining. Coal. Sci. Technol. 48 (2), 28–35. https://doi.org/10.13199/j.cnki.cst.2020.02 003 (in Chinese).
Gao, M.Z., Zhang, J.G., Li, S.W., Wang, M., Wang, Y.W., Cui, P.F., 2020d. Calculating changes in fractal dimension of surface cracks to quantify how the dynamic loading rate affects rock failure in deep mining. J. Cent. South. Univ. 27, 3013–3024.
Gao, M.Z., Xie, J., Gao, Y.N., Wang, W.Y., Xie, H.P., 2021b. Mechanical behavior of coal under different mining rates: a case study from laboratory experiments to field testing, 05 Int. J. Min. Technol. 31, 825–841. https://doi.org/10.1016/j.ijmst.2021.06.007.
Gao, M.Z., Xie, J., Guo, J., Lu, Y.Q., He, Z.Q., Li, C., 2021c. Fractal evolution and connectivity characteristics of mining-induced crack networks in coal masses at different depths. Geomech. Geophys. Geo-Energy Geo-Resour. 7 (1), 9. https://doi.org/10.1007/s40948-020-00207-4.
Gao, M.Z., Zhang, Z.L., Yin, X.G., Liu, Q., Chen, H.L., 2018. The location optimum and permeability-enhancing effect of a low-level shield rock roadway. Rock Mech. Rock Eng. 51, 2935–2948. https://doi.org/10.1007/s00603-018-1461-x.
Hartlieb, P., Leindl, M., Kuchar, F., Antretter, T., Moser, P., 2012. Damage of basalt induced by microwave irradiation. Miner. Eng. 31 (3), 82–89. https://doi.org/10.1016/j.mineng.2012.01.011.
Hartlieb, P., Toifl, M., Kuchar, F., Meisels, R., Antretter, T., 2016. Thermo-physical properties of selected hard rocks and their relation to microwave-assisted comminution. Miner. Eng. 91, 34–41. https://doi.org/10.1016/j.mineng.2015.11.008.
Hassani, F., Nekoovaght, M., NimaGharib, P., 2016. The influence of microwave irradiation on rocks for microwave-assisted underground excavation. J. Rock Mech. Geotech. Eng. 8 (1), 1–15. https://doi.org/10.1016/j.jrmge.2015.10.004.
Hong, Y.D., Lin, B.Q., Li, H., Dai, H.M., Hao, Y., 2016. Three-dimensional simulation of microwave heating coal sample with varying parameters. Appl. Therm. Eng. 93,

1145–1154. https://doi.org/10.1016/j.applthermaleng.2015.10.041.
Hu, Q., Shou, H.Z., Zeng, J., He, L., Lu, X., 2019. Comparative study on the deterioration of granite under microwave irradiation and resistance-heating treatment. Frat. Ed. Integrità Strutt. 13 (50), 638–648. https://doi.org/10.3221/IGF-ESIS.50.54.
Jiajia, C., Krishnamoorthy, P., Sohan, B., Mehrdad, N., David, J., Jeyamkondan, S., 2014. Heat and mass transport during microwave heating of mashed potato in domestic oven-model development, validation, and sensitivity analysis. J. Food Sci. 79 (10), E1991–E2004. https://doi.org/10.1111/1750-3841.12636.
Kahraman, S., Canpolat, A.N., Fener, M., 2020. The influence of microwave treatment on the compressive and tensile strength of igneous rocks. Int. J. Rock Mech. Min. Sci. 129, 104303. https://doi.org/10.1016/j.ijrmms.2020.104303.
Lek, S., Thiti, B., 2009. Mechanical property and cutting rate of microwave treated granite rock. Songklanakarin J. Sci. Technol. 31 (4), 447–452.
Li, C., Duan, L., Wu, L., Tan, S., Chikhotkin, V., 2020. Experimental and numerical analyses of electro-pulse rock-breaking drilling. J. Nat. Gas Sci. Eng. 77, 103263. https://doi.org/10.1016/j.jngse.2020.103263.
Li, H., Lin, B., Chen, Z., Hong, Y., Zheng, C., 2017a. Evolution of coal petrophysical properties under microwave irradiation stimulation for different water saturation conditions. Energy Fuels 31 (9), 8852–8864. https://doi.org/10.1021/acs.energyfuels.7b00553.
Li, J., Kaunda, R.B., Arora, S., Hartlieb, P., Nelson, P.P., 2019. Fully-coupled simulations of thermally-induced cracking in pegmatite due to microwave irradiation. J. Rock Mech. Geotech. Eng. 11 (2), 242–250. https://doi.org/10.1016/j.jrmge.2018.12.007.
Li, Y.H., Lu, G.M., Feng, X.T., Zhang, X.W., 2017b. The influence of heating path on the effect of hard rock fragmentation using microwave assisted method, 036 (006). Chin. J. Rock Mech. Eng. 1460–1468. https://doi.org/10.13722/j.cnki.jrme.2016.1229 (in Chinses).
Liang, C., Ji, H., Dou, L., Du, Y., Xu, Z., Liang, Z., Xuan, Y., Sheng, F., 2018. The characteristics of source rock and hydrocarbon charging time of Precambrian granite reservoirs in the Bongor Basin. Chad. Mar. Pet. Geol. 97, 323–338. https://doi.org/10.1016/j.marpetgeo.2018.06.003.
Lindroth, D.P., Berglund, W.R., Morrell, R.J., Blair, J.R., 1993. Microwave assisted drilling in hard rock. J R Tunn Tunni 25 (6), 24–27.
Liu, B.Q., Li, H., Chen, Z.W., Zheng, C.S., Hong, Y.D., Wang, Z., 2017. Sensitivity analysis on the microwave heating of coal: a coupled electromagnetic and heat transfer model. Appl. Therm. Eng. 126, 949–962. https://doi.org/10.1016/j.applthermaleng.2017.08.012.
Liu, S., Ni, H., Wang, Y., Zhang, H., 2021. Mechanism of multi-dimensional impact loads applied in increasing the rock cutting efficiency of a PDC bit. J. Vib. Shock 40 (2), 258–264+278. https://doi.org/10.13465/j.cnki.jvs.2021.02.035 (in Chinses).
Lu, G.M., Feng, X.T., Li, Y.H., 2019a. Experimental investigation on the effects of microwave treatment on basalt heating, mechanical strength, and fragmentation. Rock Mech. Rock Eng. 52, 2535–2549. https://doi.org/10.1007/s00603-019-1743-y.
Lu, G.M., Ting, F.X., Li, Y.H., Zhang, X.W., 2019b. The microwave-induced fracturing of hard rock. Rock Mech. Rock Eng. 52, 3017–3032. https://doi.org/10.1007/s00603-019-01790-z.
Meisels, R., Toifl, M., Hartlieb, P., Kuchar, F., Antretter, T., 2015. Microwave propagation and absorption and its thermo-mechanical consequences in heterogeneous rocks. Int. J. Miner. Process. 135 (3), 40–51. https://doi.org/10.1016/j.minpro.2015.01.003.
Menzhulin, M.G., Makhmudov, K.F., 2019. Analysis of the dependence of the breakdown point on temperature of microwave heating of loaded heterogeneous materials (rocks) based on the formation of growth of microcracks. Tech. Phys. 64 (5), 615–619. https://doi.org/10.1134/S1063784219050153.
Nekoovaght, P., Hassani, F., 2014. The influence of microwave radiation on hard rocks as in microwave assisted rock breakage applications. In: ISRM European Symposium. CRC Press-Taylor & Francis Group, Vigo, Spain.
Nicco, M., Holley, E.A., Hartlieb, P., Pfaff, K., 2020. Textural and mineralogical controls on microwave-induced cracking in granites. Rock Mech. Rock Eng. 53 (11–12), 4745–4765. https://doi.org/10.1007/s00603-020-02189-x.
Peinsitt, T., Kuchar, F., Hartlieb, P., Moser, P., Kargl, H., Restner, U., Sifferlinger, N.A., 2010. Microwave heating of dry and water saturated basalt, granite and sandstone. Int. J. Min. Miner. Eng. 2 (1), 18–29. https://doi.org/10.1504/IJMME.2010.031810, 12.
Shepel, T., Grafe, B., Hartlieb, P., Drebenstedt, C., Malovyk, A., 2018. Evaluation of cutting forces in granite treated with microwaves on the basis of multiple linear regression analysis. Int. J. Rock Mech. Min. Sci. 107, 69–74. https://doi.org/10.1016/j.ijrmms.2018.04.043.
Swart, A.J., Mendonidis, P., 2013. Evaluating the effect of radio-frequency pretreatment on granite rock samples for comminution purposes. Int. J. Miner. Process. 120 (15), 1–7. https://doi.org/10.1016/j.minpro.2013.02.002.
Toifl, M., Hartlieb, P., Meisels, R., Antretter, T., Kuchar, F., 2017. Numerical study of the influence of irradiation parameters on the microwave-induced stresses in granite. Miner. Eng. 103–104, 78–92. https://doi.org/10.1016/j.mineng.2016.09.011.
Toifl, M., Meisels, R., Hartlieb, P., Kuchar, F., Antretter, T., 2016. 3D numerical study on microwave induced stresses in inhomogeneous hard rocks. Miner. Eng. 90, 29–42. https://doi.org/10.1016/j.mineng.2016.01.001.
Wang, Z.G., Wei, Z., Han, L.J., 2013. Microwave PDC drill bit. Adv. Mater. Res. 774–776, 1414–1417. https://doi.org/10.4028/www.scientific.net/AMR.774-776.1414.
Wei, W., Shao, Z., Zhang, Y., Qiao, R., Gao, J., 2019. Fundamentals and applications of microwave energy in rock and concrete processing – a review. Appl. Therm. Eng. 157, 113751. https://doi.org/10.1016/j.applthermaleng.2019.113751.
Whittles, D.N., Kingman, S.W., Reddish, D.J., 2003. Application of numerical modelling for prediction of the influence of power density on microwave-assisted breakage. Int. J. Miner. Process. 68 (1), 71–91. https://doi.org/10.1016/S0301-7516(02)00049-2.
Xie, H.P., Liu, T., Gao, M.Z., Chen, L., Zhou, H.W., Ju, Y., Gao, F., Peng, X.B., Li, X.-J., Peng, R.D., Gao, Y.N., Li, C., He, Z.Q., Yang, M.Q., Zhao, Z.Y., 2021. Research on *in-situ* condition preserved coring and testing systems. Petrol. Sci. 18 (6), 1840–1859. https://doi.org/10.1016/j.petsci.2021.11.003.
Xie, J., Gao, M.Z., Zhang, R., Peng, G.Y., Lu, T., Wang, F., 2020. Experimental investigation on the anisotropic fractal characteristics of the rock fracture surface and its application on the fluid flow description. J. Petrol. Sci. Eng. 191, 107190. https://doi.org/10.1016/j.petrol.2020.107190.
Xue, L., Han, H., Wang, D., Liu, X.B., Yu, Z.Q., 2019. Experimental study on jet pulse assembly design and numerical simulation. Petrol. Sci. 17 (8), 222–231. https://doi.org/10.1007/s12182-019-00396-y.
Yang, X.B., Zhou, J., Yang, J.H., He, X.H., Wu, H., Gan, J., You, J.J., 2021. Natural gas and accumulation model of Mesozoic buried hill in the eastern deep water area of Qiongdongnan Basin. Acta Petrol. Sin. 42 (3), 283–292. https://doi.org/10.7623/syxb202103002 (in Chinese).
Zeng, J., Hu, Q., Chen, Y., Shu, X., Lu, X., 2019. Experimental investigation on structural evolution of granite at high temperature induced by microwave irradiation. Mineral. Petrol. 113 (3), 745–754. https://doi.org/10.1007/s00710-019-00681-z.
Zhang, W., Huang, Z., Kang, M., Shi, M.J., Zhu, Q., 2021. Research on multivariate nonlinear regression model of specific energy of rock with laser drilling based on response surface methodology. Opt Commun. 489 (4–6), 126865. https://doi.org/10.1016/j.optcom.2021.126865.
Zhang, Z.L., Liu, Y.R., Hu, Q., Ren, X.L., 2014. Integrated rock-breaking methods in well drilling. Petrol. Drill. Tech. (6), 49–52. https://doi.org/10.11911/syztjs.201406010 (in Chinese).
Zheng, Y., Ma, Z., Zhao, X., He, L., 2020. Experimental investigation on the thermal, mechanical and cracking behaviours of three igneous rocks under microwave treatment. Rock Mech. Rock Eng. 53 (8), 3657–3671. https://doi.org/10.1007/s00603-020-02135-x.
Zheng, Y.L., 2017. Fracturing of Hard Rocks by Microwave Treatment and Potential Applications in Mechanised Tunnelling. Ph.D Thesis. Monash University, Monash.
Zheng, Y.L., Ma, Z.J., Yang, S.Q., Zhao, X.B., He, L., Li, J.C., 2021. A microwave fracturability index (MFI) of hard igneous rocks. Int. J. Rock Mech. Min. Sci. 138, 104566. https://doi.org/10.1016/j.ijrmms.2020.104566.
Zheng, Y.L., Zhang, Q.B., Zhao, J., 2016. Challenges and opportunities of using tunnel boring machines in mining. Tunn. Undergr. Space Technol. 57 (aug), 287–299. https://doi.org/10.1016/j.tust.2016.01.023.
Zheng, Y.L., Zhang, Q.B., Zhao, J., 2017. Effect of microwave treatment on thermal and ultrasonic properties of gabbro. Appl. Therm. Eng. 127, 359–369. https://doi.org/10.1016/j.applthermaleng.2017.08.060.